From ribbons to nanodot arrays: nanopattern design through reductive annealing†

Palaniappan Arumugam,[a] Samuel S. Shinozaki,[a] Ruomiao Wang,[b] Guangzhao Mao[b] and Stephanie L. Brock*[a]

Received (in Berkeley, CA, USA) 13th October 2005, Accepted 3rd January 2006
First published as an Advance Article on the web 25th January 2006
DOI: 10.1039/b514595c

A new approach to the generation of nanoparticle arrays in periodic as well as non-periodic fashions has been discovered based on reduction of oxidized nanoscroll/nanoribbon precursors in the transmission electron microscope (carbothermal reduction) or by hydrogen annealing. Arrays consisting of nickel arsenide nanoparticles of size 3–4 nm have been generated.

The arrangement of nanoparticles on a substrate in periodic or non-periodic arrays is essential for their application in a number of technologically advanced devices including magnetic data storage, magnetic sensors, bio-sensors and a variety of electronic devices.[1] Periodic arrays have been generated using numerous fabrication techniques such as nanoparticle self-assembly and the use of templates both hard (*e.g.*, carbon nanotubes, anodized alumina) and soft (*e.g.*, micelles, block copolymers, proteins).[2] These methodologies routinely produce nanoparticle arrays with features on the order of a few nanometers; however, fabrication of non-periodic arrays by these methods is difficult. In contrast, lithographic and photolithographic techniques can be used to create both periodic and non-periodic structures, but producing features with dimensions of <50 nm remains a challenge, and most of the methods with these capabilities are expensive and/or have low-throughput.[3] Hence, simple techniques that permit parallel generation of non-periodic patterns of nanoparticles are desired.

It is well established that the hydrogen annealing of many bulk transition metal (TM) phosphate and arsenate phases results in the formation of corresponding transition metal phosphide and arsenide phases.[4] Additionally, we and others have shown that this approach can be used to prepare supported phosphide particles by dispersion of a precursor salt or pre-prepared phosphate nanoparticles on a substrate prior to reduction.[5,6] In the present work, we report the discovery of a simple methodology for generating nanodot arrays from the reduction of oxidized templates. In principle, this strategy can be used to create periodic or a-periodic patterns of nanoparticles, depending on the dimensions and relative orientations of the precursor particles. Additionally, we show that the original reduction method developed for the synthesis of discrete nanoparticles of phosphides[5] is also appropriate for arsenides.

The template approach described here involves the reduction of a lamellar nanoparticulate nickel arsenate adopting a ribbon or nanoscroll morphology to yield, upon volume loss, a 1-D array of nickel arsenide nanoparticles that are confined to the perimeter of the larger arsenate template. Similar reductive processes have been employed for the generation of porous metals where the monolithic structure was retained[7] or for the preparation of copper nanowires from $Cu(OH)_2$ nanobelts.[8] The process can be conducted in the transmission electron microscope (TEM) through reaction of the amorphous carbon film on the TEM grid with the arsenate precursor at elevated temperatures (carbothermal reduction), or by flowing hydrogen in a furnace (hydrogen annealing). In addition to nanopattern formation, *in situ* carbothermal reduction using the TEM has been employed to monitor the quality of the precursor material, its behavior during the transformation, the temperature required for such a transformation, and the influence of heating time on particle coalescence.

The generation of nanoparticle arrays of nickel arsenide was carried out in two steps. First, the precursor nickel arsenate layered material was synthesized using a surfactant/microemulsion assisted solvothermal method. In a typical preparation, a microemulsion containing Ni(II) was prepared by adding 1.5 mL of aqueous $NiBr_2$ (0.3 M) to a solution of cetyltrimethylammonium bromide (CTAB) in 21.1 mL *n*-hexane and 2.4 mL 1-butanol (w = [water]/[surfactant] = 39; P_0 = [alcohol]/[surfactant] = 12.2). An AsO_4^{3-} microemulsion was prepared similarly, employing aqueous $(NH_4)H_2AsO_4$. The nickel(II) microemulsion was added slowly to the arsenate microemulsion while stirring vigorously, and the 13 mL of as-formed green transparent solution was transferred to a Teflon lined autoclave (total volume of the autoclave: 23 mL) and maintained at 165 °C under autogeneous pressure for 48 h. The crude green gel was purified by several cycles of dispersing in ethanol followed by centrifugation. An ethanol dispersion of the product was then bath sonicated for an hour. The synthesized material, before and after sonication, was characterized using powder X-ray diffraction (PXRD) and TEM.

From the PXRD pattern, Fig. 1, it is evident that the product of the solvothermal reaction is single phase $Ni_3(AsO_4)_2{\cdot}H_2O$. TEM micrographs, Fig. 2a, of the non-sonicated product indicate the arsenate forms as nanoribbons with lengths varying from a few hundreds of nanometers to a few micrometers, and widths varying from 100–130 nm.

Upon sonication, the nickel arsenate ribbons curl up along the edges, Fig. 2b, to form so-called 'nanoscrolls', similar to behavior

[a]*Department of Chemistry, Wayne State University, Detroit, MI-48202, USA. E-mail: sbrock@chem.wayne.edu*
[b]*Department of Chemical Engineering and Materials Science, Wayne State University, Detroit, MI-48202, USA*

† Electronic supplementary information (ESI) available: Selected area electron diffraction pattern and list of reflections for nickel arsenide nanoparticles; X-ray powder diffraction patterns of bulk nickel arsenate reduced in H_2/Ar and carbothermally; AFM section height analysis images; notes on coalescence. See DOI: 10.1039/b514595c

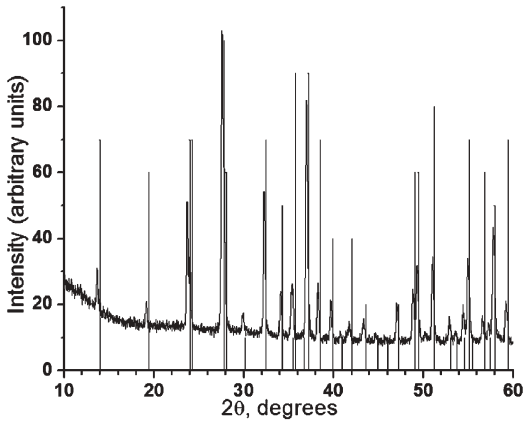

Fig. 1 The X-ray diffraction pattern of the product of the microemulsion based solvothermal reaction of nickel(II) bromide with ammonium dihydrogen arsenate. The solid lines correspond to orthorhombic $Ni_3(AsO_4)_2{\cdot}H_2O$ (ICDD PDF #32–0690). The small shift in the experimental pattern relative to the calculated pattern is due to sample displacement on the low-background holder.

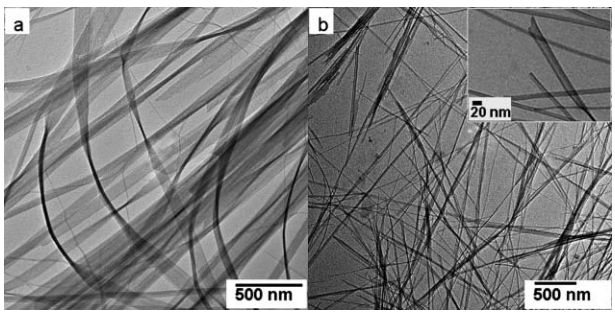

Fig. 2 TEM micrographs of $Ni_3(AsO_4)_2{\cdot}H_2O$ produced from the microemulsion based solvothermal reaction: (a) as prepared; (b) after water bath sonication for 60 min. The inset shows an HRTEM image of a partially scrolled $Ni_3(AsO_4)_2{\cdot}H_2O$ ribbon.

noted in layered materials such as graphite, metal chalcogenides, and other phosphates.[9] Although the structure of $Ni_3(AsO_4)_2{\cdot}H_2O$ has not been reported, related phases such as vivianite, kottigite, $M_3(AsO_4)_2{\cdot}8H_2O$ [M=Co, Ni], $HNiPO_4{\cdot}H_2O$ *etc.*, do exhibit layered structures,[10] and the morphology observed for our nanoparticles, as well as the behavior upon sonication, suggests that $Ni_3(AsO_4)_2{\cdot}H_2O$ is also a layered phase.

The diameter of the nanoscrolls formed after 60 min of bath sonication, *ca.* 15–20 nm (Fig. 2b), is considerably smaller than the widths of the ribbons, and the scrolls exhibit lengths ranging from 50 nm to a few micrometers. Atomic Force Microscopy (AFM) measurements of the nickel arsenate ribbons before sonication suggest a height of 2–3 nm; which, assuming an approximate nickel arsenate lamella thickness of *ca.* 0.7 nm, suggests the ribbons consist of only 3–4 arsenate layers. Sonication-induced 'scrolling' results in an apparent increase in the thickness to 4–6 nm, measured by AFM.

The second step involves reduction of the arsenate nanoscrolls to yield 1-D arrays of arsenide nanoparticles. A drop of ethanol-dispersed 60-min-sonicated nickel arsenate nanoscroll product was deposited on a carbon coated Cu grid, which was subsequently mounted on a Gatan heating stage and introduced into the TEM. The sample temperature was raised using a Gatan hot-stage controller with built-in temperature ramping program, and the progress of the *in situ* experiment was monitored by recording TEM micrographs and diffraction patterns at regular intervals and at different temperatures (300 °C, 400 °C and 420 °C). The TEM micrographs captured at 300 °C show no morphological changes: the nickel arsenate nanoscrolls remain intact. At 400 °C, the nanoscrolls start to transform into nanoparticles (Fig. 3a), and maintaining the temperature at 400 °C for a longer time (>60 min) leads to coalescence of adjacent particles and the formation of polydisperse samples (see supplementary information†). If the reduction is conducted instead at 420 °C, the complete transformation of nanoscrolls into nanoparticles occurs within 10 min of reaching 420 °C, Fig. 3b, leading to the formation of relatively uniform nanoparticles that are 3–4 nm in diameter. At longer times, coalescence again leads to particle growth (Fig. 3b, inset). The particles produced from reduction were single crystalline, exhibiting clear lattice fringes. In the inset to Fig. 3, these occur at 0.317 nm intervals, consistent with transformation of the arsenate ribbon to either $Ni_{11}As_8$ (d = 0.322 nm for the (1 0 6) reflection, 0.317 nm for the (2 1 0) reflection) or NiAs (d = 0.314 nm for the (1 0 0) reflection).

Analysis of selected area electron diffraction patterns on a field of particles suggests multiple metal-rich phases are being formed:[11] Ni_5As_2, $Ni_{11}As_8$ and NiAs; and is consistent with X-ray powder diffraction data for bulk samples of nanoribbons reduced in a H_2/Ar atmosphere or carbothermally.† There is no evidence of crystalline arsenate after *in situ* heating in the TEM. Thus, although there are many examples of morphological transformation of samples under the TEM beam, the case presented here arises distinctly from a phase transformation and the concomitant volume loss, resulting in pattern formation.

To probe further the mechanism of scroll to particle transformation, partially rolled nanoscrolls/nanoribbons of variable width were subjected to *in situ* carbothermal reduction. In the case of wider width (>300 nm) nanoribbons, Fig. 4a, the nucleation and growth started along the edges and along some streak defects. From this reaction front, particle growth and fresh nucleation occurs, moving inward from the edge, as evident from Fig. 4b. The nucleation and growth rates were considerably lower in other areas (*i.e.*, inside the ribbon) although the temperature

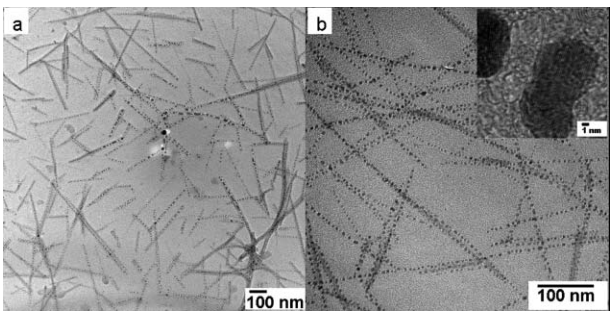

Fig. 3 TEM micrograph of the product of *in situ* carbothermal reduction of $Ni_3(AsO_4)_2{\cdot}H_2O$ at (a) 400 °C (30 min) and (b) 420 °C (10 min). The inset shows a high resolution image of a particle formed from coalescence of several adjacent smaller particles (65 min of heating, 420 °C). Lattice fringes correspond to d = 0.317 nm.

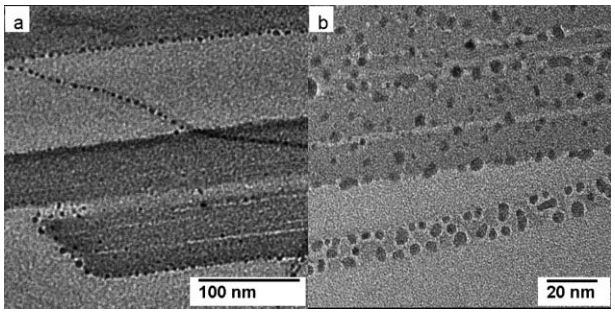

Fig. 4 *In situ* study of the transformation of arsenate nanoribbons to arsenide nanoparticles conducted at 420 °C (a) after 3 min of electron beam exposure; particle formation only at the ribbon edges, (b) after 10 min of electron beam exposure; particle formation throughout the ribbon.

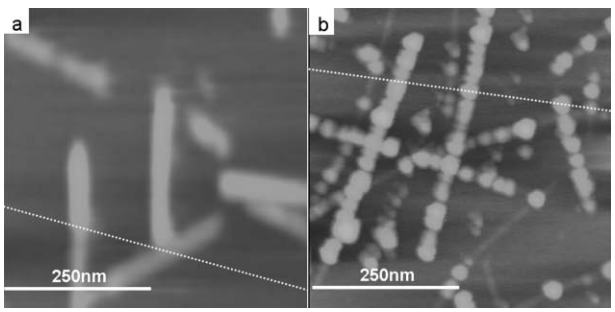

Fig. 5 AFM height images analysis: (a) $Ni_3(AsO_4)_2{\cdot}H_2O$ sonicated product; (b) product after hydrogen annealing at 425 °C for 3 h.

increase by the beam and hot stage is presumed to be uniform throughout the ribbon.

Enhanced activity at the ribbon edges is not unexpected, since dangling bonds and other defects will be concentrated in these locations. Nanoparticle formation was also found to be quicker in nanoscrolls of more narrow width (15–20 nm), and the initial particles produced, more uniform (Fig. 3). Finally, we noted that when imaging at low magnification, the nanoscroll to nanoparticle transformation was enhanced in the center of the area being imaged (*i.e.*, where the electron beam is most tightly focused, Fig. 3a). This may be due to localized heating and/or carbon sputtering by the electron beam at the elevated temperatures under which the reduction occurs.

In addition to carbothermal reduction, the arrays can also be generated by hydrogen reduction. A drop of ethanol-dispersed bath-sonicated $Ni_3(AsO_4)_2{\cdot}H_2O$ was placed on a mica substrate and imaged by Atomic Force Microscopy (AFM) in Tapping Mode. The wire-like morphology is apparent in the AFM height image, Fig. 5a, and the average thickness of the nanoscroll is calculated to be 3.9 nm from the sectional height analysis (computed along the dotted line in Fig. 5a†).

Upon hydrogen annealing at 425 °C for 3 h, the formation of a nanopattern consisting of relatively uniform sized nanoparticles is evident, Fig. 5b. The height of the particles is found to be *ca.* 4.6 nm, computed along the dotted line in Fig. 5b.† As with the carbothermal reduction, nanoparticles of nickel arsenide are formed only in those places where nanoscrolls were originally present, resulting in 1-D nanopattern formation.

The formation of 1-D nanoparticle arrays of nickel arsenide from the reduction of thin nanoribbons or nanoscrolls of nickel arsenate represents a new and potentially general methodology for arranging nanoparticles. In principle, periodic or aperiodic patterns consisting of nanoparticles of size <10 nm can be prepared by alignment or patterning of the original nanoscrolls prior to reduction. We anticipate this approach will be appropriate for generating arrays of a wide variety of metal phosphides and arsenides, as well as chalcogenides and metals; providing an oxidized precursor with appropriate morphology can be obtained.

This work was supported by the National Science Foundation (NSF DMR-0094273 and CTS 0221586) and the Institute of Manufacturing Research at Wayne State University. Electron microscopy was acquired on a JEOL 2010F purchased under NSF grant DMR-0216084 and atomic force microscopy was performed using a Dimension 3100 purchased under NSF grant CTS 0216109.

Notes and references

1 A. N. Shipway, E. Katz and I. Willner, *ChemPhysChem*, 2000, **1**, 18–52; C. R. Yonzon, D. A. Stuart, X. Zhang, A. D. McFarland, C. L. Haynes and R. P. Van Duyne, *Talanta*, 2005, **67**, 438–448.

2 B. D. Gates, Q. Xu, M. Stewart, D. Ryan, C. G. Willson and G. M. Whitesides, *Chem. Rev.*, 2005, **105**, 1171–1196; R. A. McMillan, C. D. Paavola, J. Howard, S. L. Chan, N. J. Zaluzec and J. D. Trent, *Nat. Mater.*, 2002, **1**, 247–252; R. D. Piner, J. Zhu, F. Xu, S. Hong and C. A. Mirkin, *Science*, 1999, **283**, 661–663.

3 D. Falconnet, A. Koenig, F. Assi and M. Textor, *Adv. Funct. Mater.*, 2004, **14**, 749–756; D. Wouters and U. S. Schubert, *Angew. Chem., Int. Ed.*, 2004, **43**, 2480–2495; C. L. Haynes and R. P. Van Duyne, *J. Phys. Chem. B*, 2001, **105**, 5599–5611; A. K. Raychaudhuri, *Chem. Nano Mater.*, 2004, **2**, 688–723.

4 J. Gopalakrishnan, S. Pandey and K. K. Rangan, *Chem. Mater.*, 1997, **9**, 2113–2116.

5 K. L. Stamm, J. C. Garno, G.-y. Liu and S. L. Brock, *J. Am. Chem. Soc.*, 2003, **125**, 4038–4039.

6 D. C. Phillips, S. J. Sawhill, R. Self and M. E. Bussell, *J. Catal.*, 2002, **207**, 266–273; S. J. Sawhill, K. A. Layman, D. R. Van Wyk, M. H. Engelhard, C. Wang and M. E. Bussell, *J. Catal.*, 2005, **231**, 300–313; V. Zuzaniuk and R. Prins, *J. Catal.*, 2003, **219**, 85–96; S. T. Oyama, *J. Catal.*, 2003, **216**, 343–352.

7 E. S. Toberer, A. Joshi and R. Seshadri, *Chem. Mater.*, 2005, **17**, 2142–2147; H. Yan, C. F. Blanford, J. C. Lytle, C. B. Carter, W. H. Smyrl and A. Stein, *Chem. Mater.*, 2001, **13**, 4314–4321.

8 Z. L. Wang, X. Y. Kong, X. Wen and S. Yang, *J. Phys. Chem. B*, 2003, **107**, 8275–8280.

9 L. M. Viculis, J. J. Mack and R. B. Kaner, *Science*, 2003, **299**, 1361; D. M. Kaschak, S. A. Johnson, D. E. Hooks, H.-N. Kim, M. D. Ward and T. E. Mallouk, *J. Am. Chem. Soc.*, 1998, **120**, 10887–10894; Z. Yin, Y. Sakamoto, J. Yu, S. Sun, O. Terasaki and R. Xu, *J. Am. Chem. Soc.*, 2004, **126**, 8882–8883.

10 J. L. Pizarro, M. I. Arriortua, L. Lezama, T. Rojo and G. Villeneuve, *Solid State Ionics*, 1993, **63–65**, 71–77; R. J. Hill, *Am. Mineral.*, 1979, **64**, 376–382; J. J. Melero, R. Burriel, L. Lezama, J. García-Tojal and T. Rojo, *IEEE Trans. Magn.*, 1994, **30**, 981–984; A. Goñi, J. Rius, M. Insausti, L. M. Lezama, J. L. Pizarro, M. I. Arriortua and T. Rojo, *Chem. Mater.*, 1996, **8**, 1052–1060.

11 R. D. Heyding and L. D. Calvert, *Can. J. Chem.*, 1957, **35**, 1205–1215.